



Enhanced Catalytic Performance of Carbon Nitride-Functionalized Titanium Dioxide through Efficient Oxygen Vacancy Defect Engineering for Electrochemical Recognition of Epinephrine

Chandan Saha¹ · Sarit K. Ghosh¹ · Pooja Kumari¹ · Venkata K. Perla¹ · Harishchandra Singh² · Kaushik Mallick¹

Accepted: 3 December 2023
© The Author(s) 2024

Abstract

Oxygen defect engineering is a reliable and efficient approach to modulate the electronic structure of metal oxides for the improvement of catalytic efficiency. In this work, carbon nitride supported titanium dioxide nanoparticle, with the space group of I41/amd, was prepared using a high temperature synthesis route. Transmission electron microscope study revealed that titanium dioxide particle were dispersed uniformly on the carbon nitride network. The X-ray photoelectron spectroscopy analysis predicted the formation of oxygen defects in the matrix of titanium oxide, and it also indicated the presence of titanium ions with mixed valence states. The synthesized hybrid system was evaluated as an electrocatalyst for the electrochemical detection of epinephrine using cyclic voltammetric and square wave voltammetric techniques. A custom-made device was also fabricated using synthesized hybrid material for the purpose of evaluating the electrochemical sensing of epinephrine in a pharmaceutical sample.

Keywords Oxygen defect · Titanium dioxide · X-ray photoelectron spectroscopy · Cyclic voltammetry · Epinephrine

Introduction

In the realm of advanced research, the demand for novel functional materials, characterized by low toxicity, high performance, and easy preparation, has reached a critical level of urgency. A significant amount of time and resources is being devoted by scientists and engineers to research and develop materials that exhibit a broad spectrum of versatile functions. These materials are designed to meet the increasing demand for innovative solutions in various industries, from electronics and medicine to energy and environmental protection.

Recently, graphitic carbon nitride (CN) with two dimensional structure has received much consideration as a metal-free semiconductor and is rapidly becoming a chosen material in various applications [1]. The heptazine ring structure

and the high degree of condensation enable carbon nitride to possess many advantages such as high surface area, extended catalytic durability, small bandgap, high mechanical stability and an attractive electronic structure [2]. The synthesis of carbon nitride is a one-step polymerization route from the cheap feedstocks like cyanamide [3], urea [4], thiourea [5], melamine [6] and dicyandiamide [7]. The construction of heterojunction structures has become an effective approach to improve the performance of a material [8]. Compared with single-component, heterojunction structures are beneficial to promote functional performance because of increased charge transfer through the junctions at the interfaces [9, 10].

The two-dimensional carbon nitride serves as a perfect stabilization platform for the uniform dispersion of nanomaterials without any agglomeration. A dendrite-structured α -Fe₂O₃-CN was reported for carbon dioxide reduction and found that the synergy between both the components has enhanced the reduction performance considerably [11]. Manganese oxide (α -MnO₂) supported carbon nitride was synthesized by precipitation, followed by calcination method. The composite system was applied as an electrocatalyst for the chemical hydrogenation of CO₂. The synergistic effect of both MnO₂ and carbon nitride facilitate the hydrogenation reaction with a good yield of formic acid

✉ Kaushik Mallick
kaushikm@uj.ac.za

¹ Department of Chemical Sciences, University of Johannesburg, P.O. Box: 524, Auckland Park 2006, South Africa

² Nano and Molecular Systems Research Unit, University of Oulu, FIN-90014 Oulu, Finland

[12]. The composite system of Cu_2O -carbon nitride was synthesized using a hydrothermal route and was reported for electrochemical hydrogen evolution reaction [13]. Layer structured carbon nitride with high surface area attract significant attention as electrode materials in renewable energy storage devices. Hybrid system of Zn_2GeO_4 nanoparticles and ultrathin CN layer exhibited high reversible capacity and excellent rate capability that produced the system suitable for battery application [14]. Graphitic carbon nitride incorporated MnO_2 and SnO_2 systems exhibited symmetric supercapacitor application. The specific capacitance obtained for MnO_2 -CN and SnO_2 -CN composite electrodes were 174 and 64 F.g^{-1} , respectively, as compared to the bare CN electrode 50 F.g^{-1} [15].

Titanium (TiO_2) is an abundantly occurring metal oxide with bandgap of 3.2 eV acts as a UV-active photocatalyst. The composite system of TiO_2 nanotube and carbon nitride showed superior photocatalytic activity than the individuals [16]. In another report, TiO_2 -CN system, synthesized by a thermal transformation route, exhibited the degradation of methylene blue and reduction of chromium (VI) ions. The improved photocatalytic activity of the hybrid system was due to the formation of a synergistic heterojunction that enabled a faster electron transfer at the interface between CN and TiO_2 [17]. Enhanced catalytic performance of TiO_2 -CN system for the photocatalytic oxidation of formaldehyde was reported because of the efficient space separation of photo-induced charge carriers [18]. A sensor, based on two-dimensional CuO -CN nanocomposite, fabricated by a pyrolysis technique using melamine and cupric acetate monohydrate as precursors, was reported for electrochemical detection of dopamine. The sensitivity of the sensor was attributed due to electron transfer process, where the hybrid system (CuO -CN) acted as an electron donor and the oxidized dopamine functions as an electron acceptor [19]. Graphitic carbon nitride based nanomaterials have appeared as widely applied hybrid materials that attracted interest to the scientific community due to their chemical stability, easy synthesis method, cost-effectiveness and biocompatibility. The abundance of functional amine groups and high surface area have inspired the use of carbon nitride as emerging electrochemical sensing platforms.

In this work, we report the fabrication of carbon nitride supported titanium dioxide composite system (TOCN) using a high temperature route. The hybrid system was characterized by different analytical techniques and extracted the microscopic, surface and optical properties. The synthesized system was applied as a catalyst for the electrochemical detection of epinephrine, a neurotransmitter and neuroendocrine hormone. The epinephrine detection was performed under various types of devices. The formation of oxygen vacancies in titanium dioxide facilitated the oxidation of epinephrine. This was due to the presence of oxygen-deficient

sites, which caused an unbalanced electronic structure, resulting in a rapid electron transfer between the electrode and analyte.

Experimental

Materials and Methods

Titanium isopropoxide, urea, epinephrine hydrochloride, glucose, tyrosine, urea, aminobutyric acid, valine and glutamic acid were received as analytical grade and used without further purification. All other chemicals and solvents were used as received.

Material Synthesis

Synthesis of Titanium Dioxide Titanium dioxide nanoparticles were synthesized by using a hydrothermal route according to previously reported literature [20]. In a typical synthesis process, 0.1 M of titanium isopropoxide was diluted in 20 ml of iso-propanol under continuous stirring condition and then transferred into an autoclave at 150 °C for 3 h. The solid mass was washed with deionized water, dried under vacuum at 80 °C, and subsequently calcined at 450 °C for 6 h.

Synthesis of Titanium Dioxide-Carbon Nitride (TOCN) Composite System Preformed titanium oxide and urea (1:5 ratio) were uniformly mixed and transferred to a quartz made reaction chamber. The reaction chamber was kept in a furnace at 500 °C for 4 h. At the end of the reaction, the product was collected and characterized to determine the microscopic and structural properties. The synthesized material was applied as a catalyst for the electrocatalytic detection of epinephrine. In a separate experiment, pure carbon nitride was synthesized using urea as a precursor under above mentioned reaction condition.

Electrode Preparation

The working electrode was prepared as per the following protocol. For a typical electrode preparation method, 10 mg of synthesized material (TOCN) was thoroughly grinded in presence of ethyl acetate (500 μL) to produce a slurry. A nafion solution (20 μL) was added to the slurry as a binder. A bare glassy carbon electrode (3 mm in diameter) was polished with alumina powder (0.05 μm) on the abrasive paper and rinsed with absolute ethanol and deionized water, respectively. The prepared slurry was deposited on a polished glassy carbon electrode under a heating lamp for 2 h and used as a working electrode.

Material Characterization

Microscopy study was performed using JEOL (JEM-2100) transmission electron microscope (TEM) equipped with a LaB₆ source. The X-ray diffraction (XRD) patterns were recorded on a Shimadzu XD-3A X-ray diffractometer with Cu K α radiation ($\lambda = 1.5406 \text{ \AA}$) within the diffraction angle (2θ) range from 20° to 80° . X-ray photoelectron spectra (XPS) were collected from Perkin-Elmer PHI 560 ESCA/SAM. Fourier transform infrared spectroscopy (FTIR) spectra were collected utilizing a Shimadzu IRAffinity-1. Electrochemical studies were carried out with a Bio-Logic, SP-200, potentiostat connected to a data controller. A three-electrode system was used in the experiment with a glassy carbon electrode (GCE) as the working electrode. The Ag–AgCl electrode and a Pt-electrode were used as the reference and counter electrodes, respectively. Electrochemical experiments were performed in 10 mM of phosphate buffered saline (PBS) solution, serving as the electrolyte.

Result and Discussion

The X-ray diffraction pattern (black line) of the synthesized graphitic carbon nitride (CN) supported titanium dioxide nanoparticle is shown in the Fig. 1A, within 2θ range from 20° to 80° . The overall diffraction pattern is indexed according to the anatase phase of titanium dioxide, which belongs to tetragonal structure with the space group of I4₁/amd (JCPDS: 894,921, blue bar). The inset figure shows the unit cell structure of titanium dioxide, projected along a-axis. The unit cell structure was constructed using the lattice parameter of $a=b=3.777 \text{ \AA}$, $c=9.501 \text{ \AA}$ and $\alpha=\beta=\gamma=90^\circ$. The peaks positioned at 21.5° and 26.55° belongs to (100) and (002) plane, respectively and matched according to the hexagonal phase of carbon nitride (JCPDS: 871526). The transmission electron microscopy images, Fig. 1A and B, with different magnifications, show the titanium dioxide particle (dark spots) within the graphitic carbon nitride network.

To identify the formation of carbon nitride (CN) during the synthesis of TOCN, an infrared analysis technique was performed. Figure 2 shows the Fourier-transform infrared (FTIR) spectra of CN and TOCN, which suggests the existence of condensed aromatic carbon–nitrogen heterocycles. In the CN sample, the overall feature in the IR-spectrum is identical to those already reported in the literature [21]. The vibrational bands at 1623 and 1555 cm^{-1} are attributed to C=N stretching, while the bands at 1407 , 1321 and 1236 cm^{-1} correspond to aromatic C–N stretching mode. All the above mentioned signatures are also visible in the TOCN sample, indicates the formation of carbon nitride. The triazine ring mode, correspond to condensed carbon–nitrogen heterocycles, detected at

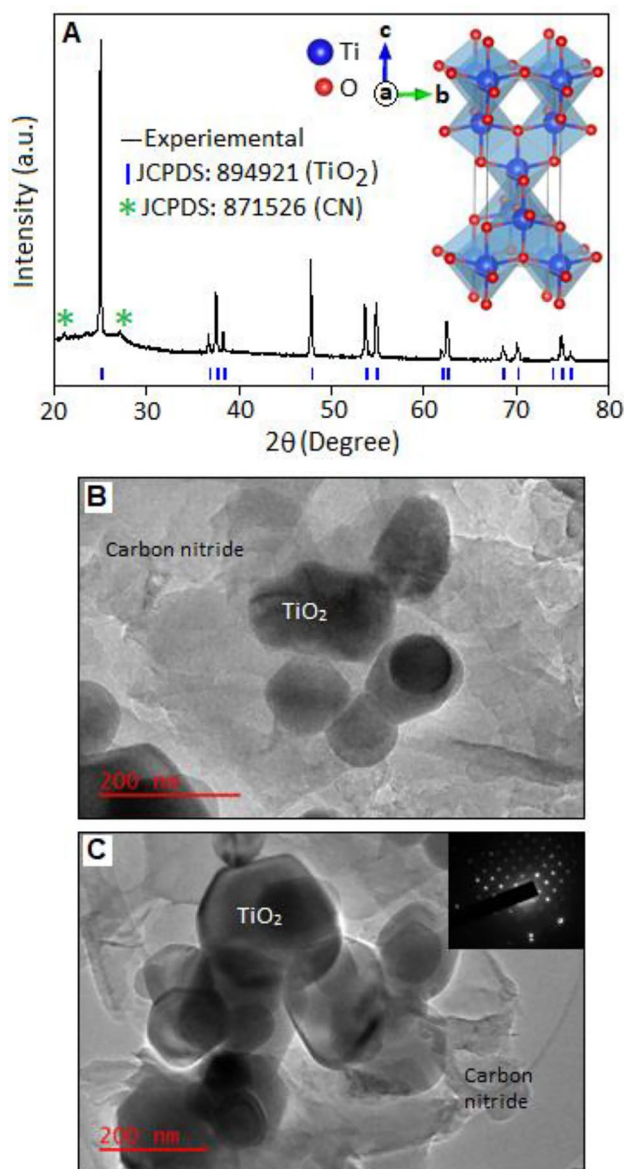


Fig. 1 A X-ray diffraction pattern (black line) of the graphitic carbon nitride supported titanium dioxide, with the unit cell representation of titanium dioxide (projected along a-axis). **B** and **C** TEM images of graphitic carbon nitride supported titanium dioxide under different magnifications. Dark spots indicate the presence of titanium dioxide nanoparticles. The inset figure **C** shows the selected area electron diffraction pattern

804 cm^{-1} for both the samples with different intensities [21, 22]. In the IR signal, the broad bands within the range of $3000\text{--}3500 \text{ cm}^{-1}$ are also visible for both the samples (CN and TOCN) correspond to the stretching modes of the amine groups, such as, $-\text{NH}_2$ or $=\text{NH}$.

The X-ray photoelectron spectroscopy (XPS) technique was applied to analyse the elemental composition of the carbon nitride supported titanium dioxide (TOCN) system.

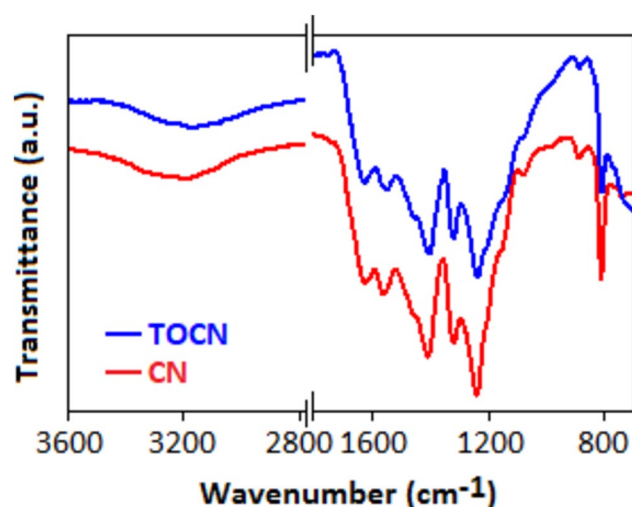


Fig. 2 Fourier-transform infrared spectra of CN and TOCN

Figure 3A shows the survey scan within the ranges from 0 to 900 eV and the spectrum displayed the presence of elements, such as Ti, O, C, and N. A high resolution deconvoluted spectrum of Ti 2p is illustrated in Fig. 3B. In this spectrum, the doublet Ti 2p_{3/2} and Ti 2p_{1/2} with the binding energy values 458.6 and 464.8 eV was noticed, originated from spin orbit-splitting, consistent with Ti⁴⁺ in TiO₂ lattice [23]. In the deconvoluted spectrum, the appearance of another peak at the binding energy 461.1 eV correspond to Ti³⁺ [24], indicate the presence of titanium ion with mixed valence state. Broad (~6 eV) O 1s spectrum, Fig. 3C, was deconvoluted with Gaussian peak fit, which produced two components centred at 530.5 and 531.6 eV. The peak, positioned at 530.5 eV, attributed to the surface lattice oxygen of TiO₂, whereas the higher binding energy peak at 531.6 eV ascribed as oxygen defects in the matrix of metal oxide, related to oxygen vacancies [25, 26]. In general, four approaches have been adopted to create oxygen vacancies in the structure, (a) control over the synthesis, (b) atom substitution, (c) surface modification (through doping) and (d) in situ surface treatment [27]. In the current synthesis approach, during the formation of carbon nitride at high temperature, in presence of TiO₂, oxygen vacancies were created at the matrix of metal oxide system. High resolution C 1s spectrum, Fig. 3D, deconvoluted into main intensity peak positioned at 288.4 eV, originated from N – C = N in the triazine unit and a diffuse peak at 284.8 eV is related to the C–C bond in the graphitic carbon nitride system [28]. The deconvoluted spectra of N 1s, Fig. 3E, shows two prominent peaks at ~398.8 eV and ~400.4 eV, originated from the nitrogen of triazine ring and primary amine (–NH₂) group of carbon nitride matrix [29].

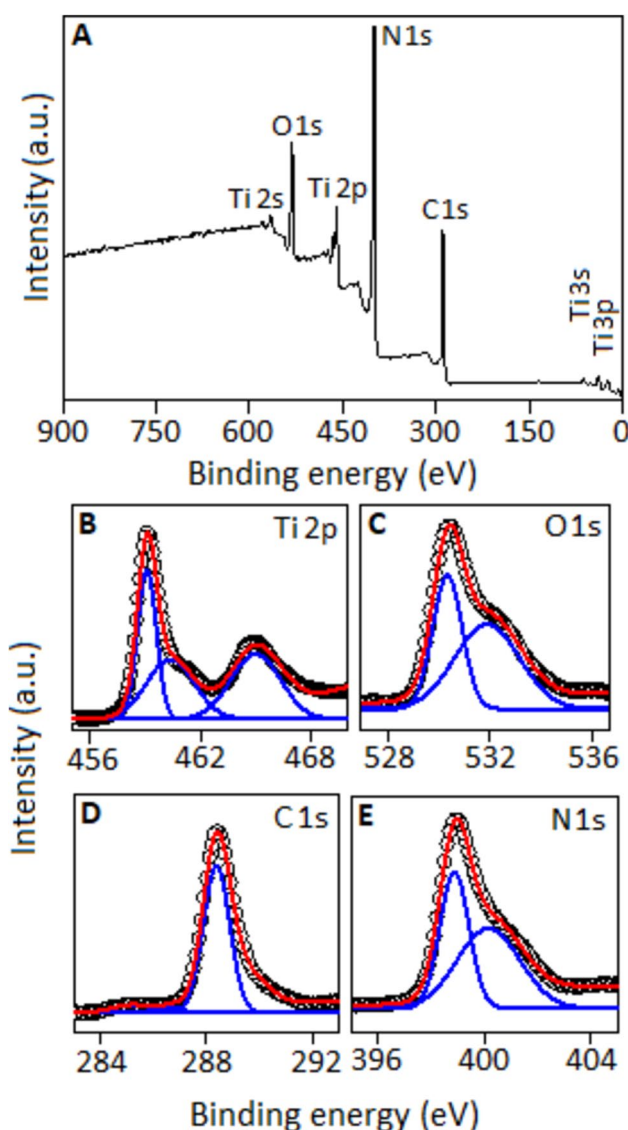


Fig. 3 A The XPS survey spectrum of carbon nitride supported titanium dioxide (TOCN) system. High resolution deconvoluted spectrum of Ti 2p B, O 1s C, C 1s D and N 1s E

Application of TOCN for the Electrochemical Detection of Epinephrine

Using a Conventional Electrochemical Cell

For the electrochemical detection of epinephrine, the cyclic voltammetry (CV) technique was applied in the presence of PBS electrolyte (6.0 mL) under the scan rate of 50 mVs⁻¹ within the voltage range from -0.1 to 0.8 V. To study the electrochemical detection of epinephrine, we have used both titanium dioxide and TOCN as a working electrode modifier. Figure 4A shows the cyclic voltammograms for bare GCE in absence of epinephrine and the corresponding

voltammogram (a) shows the current value of $0.17 \mu\text{A}$ at 0.28 V . An increased current value $0.47 \mu\text{A}$ at 0.28 V was observed for bare GCE in presence of epinephrine ($20 \mu\text{M}$), voltammogram (b), indicates the oxidation of the analyte on the electrode surface. It is also important to mention that titanium dioxide modified GCE did not exhibit considerable enhancement of current response in presence of epinephrine ($20 \mu\text{M}$), voltammogram (c), whereas TOCN modified GCE displayed a well-defined peak with the current value of $0.9 \mu\text{A}$ at 0.28 V in presence of epinephrine ($20 \mu\text{M}$), indicated improved catalytic oxidation of the analyte. In the TOCN sample, the formation of oxygen vacancy, as evidenced by XPS study, could be responsible for the improved electrocatalytic oxidation of epinephrine. It is well documented in the literature that the creation of oxygen vacancy has recognized as an effective strategy to prepare high-performance catalysts for the oxidation of organic compounds, photoelectrochemical reactions, supercapacitor application and water oxidation because the oxygen-deficient sites can lead to an unbalanced electronic structure, resulting in rapid electron transfer [25–27, 30, 31]. The oxygen vacancies serve as shallow donors that effectively enhanced electronic and photoelectrochemical properties of Fe_2O_3 nanostructures [32–34]. Similarly, oxygen vacancies in $\alpha\text{-Fe}_2\text{O}_3$ nanorods improved its donor density that facilitate the electrochemical performance for supercapacitor application [25].

Figure 4B shows a steady increase of current values with increasing concentration of epinephrine for the TOCN modified GCE electrode. In absence of epinephrine, the current value $0.40 \mu\text{A}$ at 0.28 V was noticed. The maximum current value was reached to $1.3 \mu\text{A}$ for the epinephrine concentration $50 \mu\text{M}$ with a prominent anodic peak at 0.28 V . The increase of anodic peak current, with increasing epinephrine concentration, indicate enhanced electron transfer through the defect sites of titanium dioxide. The sensitivity value for the detection of epinephrine using cyclic voltametric technique was obtained $0.255 \mu\text{A} \cdot \mu\text{M}^{-1} \cdot \text{cm}^{-2}$. The detection of epinephrine was further verified using square-wave voltammetry technique, which is considered as the second generation of pulse technique with higher sensitivity and rapid measurement [35]. Similar results were also observed in the square wave voltammetry technique, Fig. 4C, where the increase of current value was noticed with increasing epinephrine concentration with the sensitivity value of $2.26 \mu\text{A} \cdot \mu\text{M}^{-1} \cdot \text{cm}^{-2}$.

The chronoamperometric response of the TOCN modified electrode towards the subsequent addition of epinephrine was further assessed under the optimized experimental condition. Figure 5A, shows the amperometric response (current as a function of time) of epinephrine at 0.25 V . As documented in the figure, the amperometric

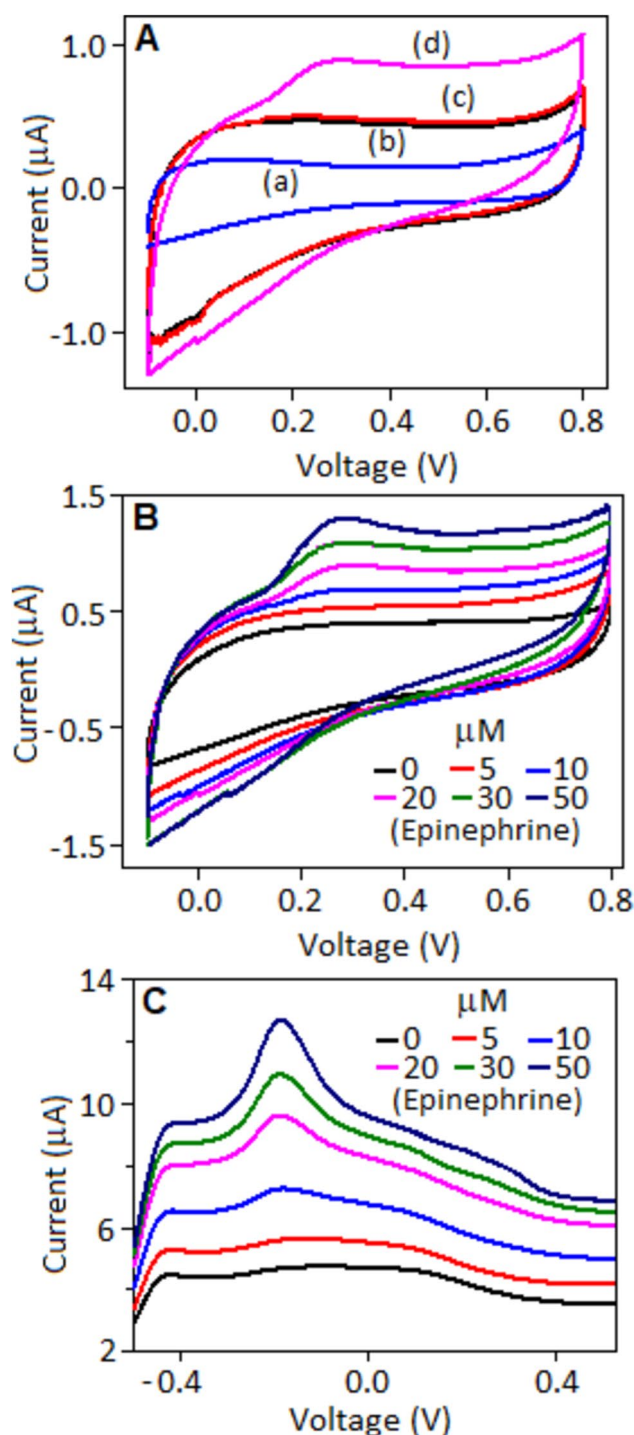


Fig. 4 A Cyclic voltammograms for bare GCE in the absence of epinephrine (curve 'a'), bare GCE in presence of epinephrine, $20 \mu\text{M}$ (curve 'b'), titanium dioxide modified GCE in presence of epinephrine, $20 \mu\text{M}$ (curve 'c') and TOCN modified GCE in presence of epinephrine, $20 \mu\text{M}$ (curve 'd'), B Cyclic voltammograms for TOCN modified GCE with increasing concentration of epinephrine, C Square-wave voltammograms for TOCN modified GCE with increasing concentration of Epinephrine

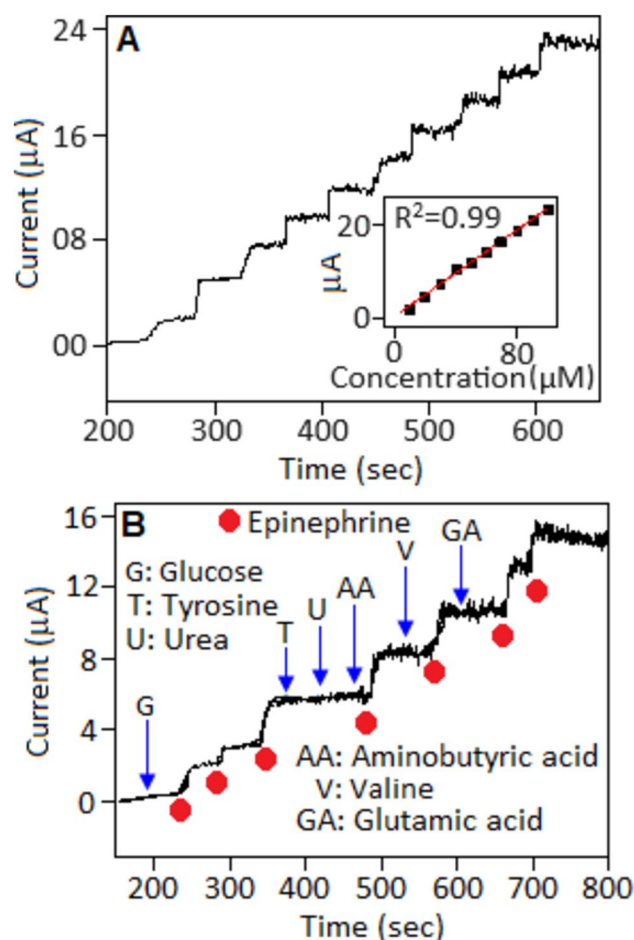


Fig. 5 **A** Amperometric response of TOCN modified GCE on successive addition of 10 μL of epinephrine in every 40 s time interval with an applied potential of 0.25 V. Inset: the calibration plot of current response with varying epinephrine concentrations. **B** The addition of interferences species (glucose, tyrosine, urea, aminobutyric acid, valine and glutamic acid, 50 μL each) show the irresponsive nature towards the amperometric current signal

signal showed a good linear correlation and a stepwise increase of current value for every addition of epinephrine (10 μM), within the range from 10 μM to 100 μM in every 40 s time interval. The calibration plot of current response with varying concentration of epinephrine is displayed in Fig. 5A, inset. The regression coefficient and sensitivity values, within the time interval from 200 to 660 s, are 0.99822 and $3.1196 \mu\text{A} \mu\text{M}^{-1} \cdot \text{cm}^{-2}$, respectively. The TOCN modified electrode showed tolerance towards other analytes including glucose, tyrosine, urea, aminobutyric acid, valine and glutamic acid, 50 μM each, Fig. 5B. The absence of a substantial current alteration upon the introduction of the aforementioned analytes signifies the selectivity of TOCN towards epinephrine.

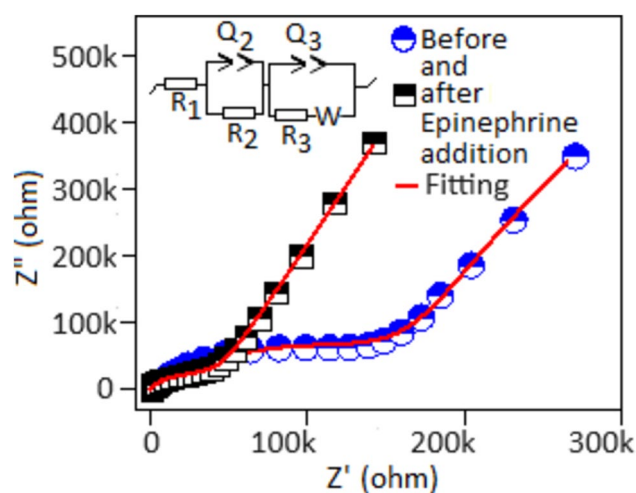
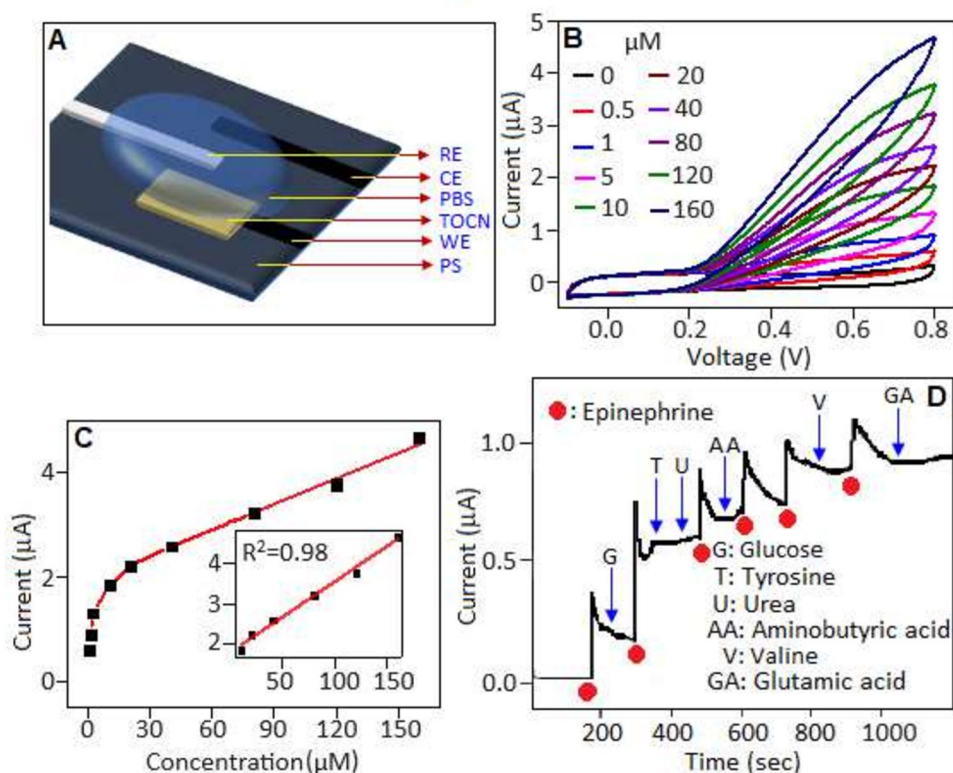


Fig. 6 Electrochemical impedance spectra of TOCN modified GCE before and after the addition of epinephrine within the frequency range from 1.0 MHz to 1.0 mHz

Electrochemical Impedance Characteristics of the TOCN Modified Electrode

Figure 6, main panel, illustrates the Nyquist plots that depict the electrochemical impedance characteristics of the TOCN based electrode before and after the exposure to epinephrine within the range from 200 kHz to 100 mHz. The electrochemical impedance spectroscopy exhibited two distinct regions. The higher frequency region displayed a semicircular shape, governed by electrode reaction kinetics (charge transfer) process. On the other hand, the lower frequency range exhibited a linear characteristics, suggesting a diffusion-controlled process. The diameter of the semi-circle represents the charge transfer resistance that provide the insight of electron transfer kinetics at the electrode–electrolyte interface during the electrochemical process. The electrochemical impedance analysis revealed a significant changes in charge transfer resistance value, which was 162 k Ω (before the addition of epinephrine) and decreased to 56.35 k Ω (after the addition of epinephrine), indicating a facile approach of epinephrine on the surface of TOCN system. The Nyquist plots are modelled according to the equivalent circuit diagram, Fig. 6, inset, and the summarized values of the fitting parameters are shown in Table S1, supplementary information. The diagram constant of two components (R_2Q_2 and R_3Q_3) connected in series combination. The addition of epinephrine causes a significant shift in the semicircular arc pattern. Such a behavior is associated with the faster charge transfer process between electrode and electrolyte interface and that leads to decrease in the resistance values (R_1 , R_2 and R_3) of the device. The R_1 , R_2 , and R_3 represent equivalent series resistance, charge transfer

Fig. 7 **A** Schematic diagram of the custom made device. **B** Cyclic voltammogram of different concentrations of epinephrine (0.0–160 μM). **C** Graphical representation of current as a function of epinephrine concentration (0.5–160 μM). Inset: the calibration plot of current response with varying epinephrine concentrations. **D** The addition of interferences species (glucose, tyrosine, urea, aminobutyric acid, valine and glutamic acid, 20 μM each) show the irresponsive nature towards the amperometric current signal



resistance and leakage resistance, respectively. The low-frequency region deviates from the ideal capacitive trend and could be attributed to the leakage resistance (R_3) in parallel with the leakage capacitance (Q_3). Ion diffusion mechanism between electrode and electrolyte interface leads to Warburg impedance (W), which is connected in series with R_3 .

Detection of Epinephrine Using a Custom Made Electrochemical Device

A conducting graphitic pencil was applied to draw the working electrode (WE) and counter electrode (CE), 1 mm \times 15 mm, each, 10 mm apart, on a piece of paper, supported on a glass slide. A thin-line was drawn in between WE and CW electrodes using silver paint, acted as a reference electrode (RE). A thin film of the synthesized material (TOCN) was deposited on the WE. 100 μL of PBS solution

was deposited on the device to connect the working, counter, and reference electrodes, Fig. 7A. Figure 7B displayed the cyclic voltammogram of different concentrations of epinephrine within the range from 0.5 to 160 μM . Figure 7C shows the graphical representation of current as a function of epinephrine concentration. The calibration plot, Fig. 7C, inset, shows the current response with varying concentration of epinephrine. The sensitivity of the device was achieved 0.1122 $\mu\text{A}\mu\text{M}^{-1}\cdot\text{cm}^{-2}$ within the range from 10 to 160 μM (analyte concentration). Chronoamperometric study was performed by adding 10 μM epinephrine under different time interval between 100 to 1200 s, Fig. 7D. Sharp increase of current responses were noticed after every addition of the epinephrine (10 μM), whereas no significant changes in current value was observed during the addition of analytes like glucose, tyrosine, urea, aminobutyric acid, valine and glutamic acid, 20 μM each, indicates selectivity of the TOCN catalyst for epinephrine detection in custom made device.

Table 1 Selective determination of epinephrine in pharmaceutical sample

Sample	Added (μM)	Found (μM)	Relative error (%)	RSD (%) (3 measurements)	Recovery (%)
Epinephrine injection solution (Epipen®)	10	9.8	2	0.25	98
	20	20.3	1.5	0.21	101.5
	30	29.5	1.66	0.22	98.33

RSD relative standard deviation

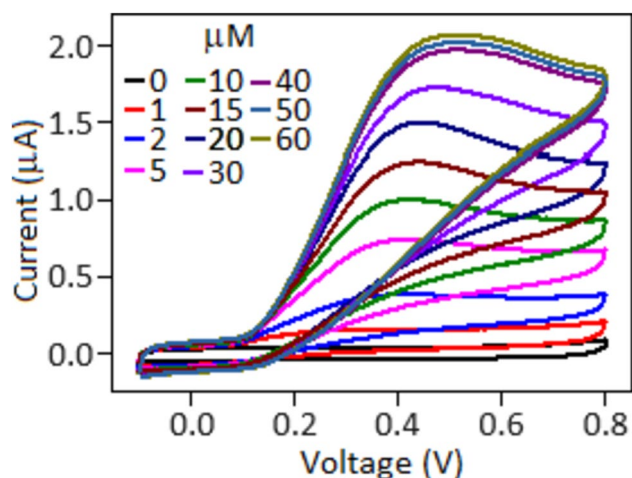


Fig. 8 Cyclic voltammograms of different concentrations of epinephrine (0.0–60 μM) using a screen printed electrode

Detection of Epinephrine in Pharmaceutical Sample

To verify the practical applicability of the custom-made device, it was utilized to determine the concentration of epinephrine in commercial injection, Epipen[®]. The as fabricated electrochemical cell was introduced with the epinephrine injection solution with the concentrations of 10 μM , 20 μM , and 30 μM . The cyclic voltammogram of the device was recorded and the results have been shown in the Table 1.

The results showed good performance of the electrocatalyst that emphasized the reliability of the device to detect the samples in an accurate manner.

Detection of Epinephrine Using a Screen Printed Electrode

Screen printed electrodes are widely recognized for their significance in the field of electrochemistry. The major advantages of the screen printed electrodes are cost-effectiveness and adaptability for miniaturization. Screen printed electrodes have extensive use in point-of-care diagnostics, which makes them indispensable in healthcare and pharmaceutical applications [36–38]. The electrochemical detection of epinephrine was further performed on a screen printed electrode (SPE), Metrohm, DropSen DRP-C110, using TOCN as a catalyst. Figure 8 displays the cyclic voltammograms of the TOCN modified screen printed electrode for various concentrations of epinephrine. An increase in current value was noticed with addition of epinephrine. The voltammograms shows a steady current response from 1 to 40 μM and subsequently a saturation point was reached, as evidenced by the voltammogram. It is also important to mention that the custom made device is more sensitive for wider range of epinephrine detection as compared with the conventional electrochemical cell and commercial screen printed electrode.

A comparison table shows the electrochemical recognition of epinephrine under different catalytic conditions, Table 2, [39–47].

Table 2 Comparison of epinephrine detection under different catalytic conditions

Electrode and sensing material	Sensitivity ($\mu\text{A} \cdot \mu\text{M}^{-1} \cdot \text{cm}^{-2}$)	LOD (μM)	Linear range (μM)	Ref
CPE: EDDPT/GO	-	0.65	1.5–600	[39]
GCE: Gr/Au nanocomposites	-	0.007	0.05–8	[40]
GCE: PEDOT-AuNPs	0.021	1.4	-	[41]
GCE: Catechol	0.6	1.6	5–80 & 80–900	[42]
GCE: Chit-CNT	-	0.03	0.05–10	[43]
GCE: Pd-Au nanoparticles	-	5	50–260	[44]
GCE: MGO	-	0.13	100–600	[45]
CPE: 2-Hydrobenzimidazole	-	3	-	[46]
GCE: OMC-NiO	-	0.085	0.8–50	[47]
GCE: TOCN	0.255	1	4–50	This work
Custom-made device: TOCN	0.1122	0.5	10–160	This work

CPE Carbon Paste Electrode, CV Cyclic voltammetry, SWV Square wave voltammetry, GCE Glassy carbon electrode, Gr-Au Graphene-gold, EDDPT 2-(5-Ethyl-2,4-dihydroxyphenyl)-5,7-dimethyl-4H-pyrido[2,3-d][1,3]thiazine-4-one, GO Graphene oxide, Chit-CNT Multiwall carbon nanotube–chitosan biopolymer nanocomposite, Pd-Au Palladium-gold, MGO Melamine modified graphene oxide, OMC-NiO Ordered mesoporous carbon/Nickle Oxide, LOD limit of detection

Conclusion

Here we report a simple method to create the oxygen vacancy in titanium dioxide by applying an oxygen vacancy defect engineering strategy to prepare a high-performance catalyst for the efficient electrochemical recognition of epinephrine. The catalyst, carbon nitride supported titanium dioxide nanoparticle, was synthesized by applying a high temperature route. The X-ray photoelectron spectroscopy analysis predicted the formation of oxygen vacancies in the matrix of titanium dioxide nanoparticle. The oxygen-deficient sites led to the creation of an unbalanced electronic structure, which, in turn, caused rapid electron transfer and facilitated the oxidation of epinephrine. The synthesized hybrid system presented the sensitivity values of 0.255 and $2.26 \mu\text{A} \mu\text{M}^{-1} \text{cm}^{-1}$ for the electrochemical detection of epinephrine using cyclic voltammetric and square wave voltammetric techniques, respectively, applying glassy carbon as working electrodes. A custom made device was also fabricated based on hybrid catalyst to evaluate the sensing performance of epinephrine in pharmaceutical sample. The findings mentioned above suggest that carbon nitride-supported titanium dioxide has the potential to serve as a catalyst for the electrochemical detection of epinephrine.

Supplementary Information The online version contains supplementary material available at <https://doi.org/10.1007/s12678-023-00860-9>.

Acknowledgements This study was supported by the Faculty of Science, University Research Council and the Global Excellence and Stature program 4.0, University of Johannesburg.

Author Contributions CS: Conceptualization, Validation, Investigation, Draft writing; SKG: Material characterization and draft writing; PK: Material characterization; VKP: Material synthesis and characterization; HCS: XPS analysis; KM: Conceptualization, Resources, Supervision, Writing.

Funding Open access funding provided by University of Johannesburg. This study was funded through Faculty of Science and the Global Excellence and Stature program 4.0, University of Johannesburg.

Data Availability Not applicable.

Declarations

Conflict of Interest The authors declare no conflict of interest.

Ethical Approval Not applicable.

Open Access This article is licensed under a Creative Commons Attribution 4.0 International License, which permits use, sharing, adaptation, distribution and reproduction in any medium or format, as long as you give appropriate credit to the original author(s) and the source, provide a link to the Creative Commons licence, and indicate if changes were made. The images or other third party material in this article are included in the article's Creative Commons licence, unless indicated otherwise in a credit line to the material. If material is not included in the article's Creative Commons licence and your intended use is not

permitted by statutory regulation or exceeds the permitted use, you will need to obtain permission directly from the copyright holder. To view a copy of this licence, visit <http://creativecommons.org/licenses/by/4.0/>.

References

1. Z. Zhao, Y. Sun, F. Dong, Graphitic carbon nitride based nanocomposites: a review. *Nanoscale* **7**, 15–37 (2015)
2. X. Wang, K. Maeda, A. Thomas, A metal-free polymeric photocatalyst for hydrogen production from water under visible light. *Nat. Mater.* **8**, 76–80 (2009)
3. K. Takanabe, K. Kamata, X. Wang, M. Antonietti, J. Kubota, K. Domen, Photocatalytic hydrogen evolution on dye-sensitized mesoporous carbon nitride photocatalyst with magnesium phthalocyanine. *Phys. Chem. Chem. Phys.* **12**, 13020–13025 (2010)
4. F. Dong, L. Wu, Y.J. Sun, M. Fu, Z. Wu, S. Lee, Efficient synthesis of polymeric g-C₃N₄ layered materials as novel efficient visible light driven photocatalysts. *J. Mater. Chem.* **21**, 15171–15174 (2011)
5. Y. Zhang, J. Liu, G. Wu, W. Chen, Porous graphitic carbon nitride synthesized via direct polymerization of urea for efficient sunlight-driven photocatalytic hydrogen production. *Nanoscale* **4**, 5300–5303 (2012)
6. S. Yan, Z. Li, Z. Zou, Photodegradation of rhodamine B and methyl orange over boron-doped g-C₃N₄ under visible light irradiation. *Langmuir* **26**, 3894–3901 (2010)
7. G. Zhang, J. Zhang, M. Zhang, X. Wang, Polycondensation of thiourea into carbon nitride semiconductors as visible light photocatalysts. *J. Mater. Chem.* **22**, 8083–8091 (2012)
8. S. Jiang, K. Zhou, Y. Shi, S. Lo, H. Xu, Y. Hu, Z. Gui, In situ synthesis of hierarchical flower-like Bi₂S₃/BiOCl composite with enhanced visible light photocatalytic activity. *Appl. Surf. Sci.* **290**, 313–310 (2014)
9. S. Hu, L. Yang, Y. Tian, X. Wei, J. Ding, J. Zhong, P. Chu, Non-covalent doping of graphitic carbon nitride with ultrathin graphene oxide and molybdenum disulfide nanosheets: An effective binary heterojunction photocatalyst under visible light irradiation. *J. Colloid Interface Sci.* **431**, 42–49 (2014)
10. M. Yan, Y. Wu, Y. Yan, X. Yan, F. Zhu, Y. Hua, W. Shi, Synthesis and Characterization of Novel BiVO₄/Ag₃VO₄ Heterojunction with Enhanced Visible-Light-Driven Photocatalytic Degradation of Dyes. *ACS Sustainable Chem. Eng.* **4**, 757–766 (2016)
11. Y. Shen, Q. Han, J. Hu, W. Gao, L. Wang, L. Yang, C. Gao, Q. Shen, C. Wu, X. Wang, X. Zhou, Y. Zhou, Z. Zou, Artificial trees for artificial photosynthesis: construction of dendrite-structured $\alpha\text{-Fe}_2\text{O}_3/\text{g-C}_3\text{N}_4$ Z-Scheme system for efficient CO₂ reduction into solar fuels. *ACS Appl. Energy Mater.* **3**, 6561–6572 (2020)
12. B. Mulik, A. Munde, B. Bankar, A. Biradar, B. Sathe, Highly efficient manganese oxide decorated graphitic carbon nitride electrocatalyst for reduction of CO₂ to formate. *Catal. Today* **370**, 104–113 (2021)
13. A. Paul, A. Sajeev, R. Nivetha, K. Gothandapani, P. Bhardwaj, K. Govardhan, V. Raghavan, G. Jacob, R. Sellapan, S. Jeong, A. Grace, Cuprous oxide (Cu₂O)/graphitic carbon nitride (g-C₃N₄) nanocomposites for electrocatalytic hydrogen evolution reaction. *Diam. Relat. Mater.* **107**, 107899 (2020)
14. X. Li, Y. Feng, M. Li, W. Li, H. Wei, D. Song, Smart Hybrids of Zn₂GeO₄ Nanoparticles and Ultrathin g-C₃N₄ Layers: Synergistic Lithium Storage and Excellent Electrochemical Performance, **25**, 6858–6866 (2015)
15. J. Kavil, P. Anjana, P. Periyat, R. Rakhi, One-pot synthesis of g-C₃N₄/MnO₂ and g-C₃N₄/SnO₂ hybrid nanocomposites for supercapacitor applications. *Sustain.* **2**, 2244–2251 (2018)
16. X. Zhou, B. Jin, L. Li, F. Peng, H. Wang, H. Yu, Y. Fang, A carbon nitride/TiO₂ nanotube array heterojunction visible-light

- photocatalyst: synthesis, characterization, and photoelectrochemical properties. *J. Mater. Chem.* **22**, 17900–17905 (2012)
17. K. Sridharan, E. Jang, T. Park, Novel visible light active graphitic C₃N₄-TiO₂ composite photocatalyst: synergistic synthesis, growth and photocatalytic treatment of hazardous pollutants. *Appl. Catal. B* **142**, 718–728 (2013)
 18. J. Yu, S. Wang, J. Low, W. Xiao, Enhanced photocatalytic performance of direct Z-scheme g-C₃N₄-TiO₂ photocatalysts for the decomposition of formaldehyde in air. *Phys. Chem. Chem. Phys.* **15**, 16883–16890 (2013)
 19. J. Zou, S. Wu, Y. Liu, Y. Sun, Y. Cao, J. Hsu, A. Wee, J. Jiang, An ultra-sensitive electrochemical sensor based on 2D g-C₃N₄/CuO nanocomposites for dopamine detection. *Carbon* **130**, 652–663 (2018)
 20. M. Aravind, M. Amalanathan, M. Mary, Synthesis of TiO₂ nanoparticles by chemical and green synthesis methods and their multifaceted properties. *SN Appl. Sci.* **408**, 3 (2021)
 21. M. Kim, S. Hwang, J. Yu, Novel ordered nanoporous graphitic C₃N₄ as a support for Pt-Ru anode catalyst in direct methanol fuel cell. *J. Mater. Chem.* **17**, 1656–1959 (2007)
 22. T. Komatsu, Prototype carbon nitrides similar to the symmetric triangular form of melon. *J. Mater. Chem.* **11**, 802–803 (2001)
 23. B. Bharti, S. Kumar, H. Lee, R. Kumar, Formation of oxygen vacancies and Ti³⁺ state in TiO₂ thin film and enhanced optical properties by air plasma treatment. *Sci. Rep.* **6**, 32355 (2016)
 24. I. Bertóti, M. Mohai, J. Sullivan, S. Saied, Surface characterisation of plasma-nitrided titanium: an XPS study. *Appl. Surf. Sci.* **84**, 357–371 (1995)
 25. X. Lu, Y. Zeng, M. Yu, T. Zhai, C. Liang, S. Xie, M. Balogun, Y. Tong, Oxygen-deficient hematite nanorods as high-performance and novel negative electrodes for flexible asymmetric supercapacitors. *Adv. Mater.* **26**, 3148–3155 (2014)
 26. J. Gan, X. Lu, J. Wu, S. Xie, T. Zhai, M. Yu, Z. Zhang, Y. Mao, S. Wang, Y. Shen, Y. Tong, Oxygen vacancies promoting photoelectrochemical performance of In₂O₃ nanocubes. *Sci. Rep.* **3**, 1021 (2013)
 27. P. Wang, X. Ma, X. Hao, B. Tang, A. Abudula, G. Guan, Oxygen vacancy defect engineering to promote catalytic activity toward the oxidation of VOCs: a critical review. *Catal. Rev. Sci.* **1**–54, (2022)
 28. W. Wang, H. Zhang, S. Zhang, Y. Liu, G. Wang, C. Sun, H. Zhao, Potassium ion assisted regeneration of active Cyano-groups in carbon nitride nanoribbons: visible light driven photocatalytic nitrogen reduction. *Angew. Chem. Int. Ed.* **58**, 2–9 (2019)
 29. E. Alwin, W. Nowicki, R. Wojcieszak, M. Zieliński, M. Pietrowski, Elucidating the structure of the graphitic carbon nitride nanomaterials via X-ray photoelectron spectroscopy and X-ray powder diffraction techniques. *Dalton Trans.* **49**, 12805–12813 (2020)
 30. J. Liu, H. Tang, P. Jian, B. Liu, Oxygen-vacancy defect engineering to boost the aerobic oxidation of limonene over Co₃O₄ nanocubes. *Appl. Catal. B Environ.* **334**, 122828 (2023)
 31. S. Corby, L. Francàs, A. Kafizas, J. Durrant, Determining the role of oxygen vacancies in the photoelectrocatalytic performance of WO₃ for water oxidation. *Chem. Sci.* **11**, 2907–2914 (2020)
 32. T. Lindgren, H. Wang, N. Beermann, L. Vayssieres, A. Hagfeld, S. Lindquist, Aqueous photoelectrochemistry of hematite nanorod array. *Sol. Energy Mater. Sol. C* **71**, 231 (2002)
 33. G. Wang, Y. Ling, D. Wheeler, K. George, K. Horsley, C. Heske, J. Zhang, Y. Li, Facile Synthesis of Highly Photoactive α -Fe₂O₃-Based Films for Water Oxidation. *Nano Lett.* **11**, 3503–3509 (2011)
 34. Y. Ling, G. Wang, J. Reddy, C. Wang, J. Zhang, Y. Li, The Influence of Oxygen Content on the Thermal Activation of Hematite Nanowires. *Angew. Chem. Int. Ed.* **124**, 4150–4155 (2012)
 35. V. Yadav, M. Raj, R. Goyal, Comparison of different unmodified and nano-material modified sensors for the ultrasensitive determination of serotonin. *J. Electrochem. Soc.* **167**, 027539 (2020)
 36. B. Sriram, J. Baby, Y. Hsu, S. Wang, M. George, Scheelite-type rare earth vanadates TVO₄ (T= Ho, Y, Dy) electrocatalysts: Investigation and comparison of T site variations towards bifunctional electrochemical sensing application. *J. Chem. Eng.* **451**, 138694 (2023)
 37. T.S.K. Sharma, J. Jana, K. Bhamu, J. Song, S. Sivaselvam, T. Van Tam, S. Kang, J. Chung, S. Hur, W. Choi, Rational synthesis of alkaline earth metal vanadates: Structural origin of MgVO₃ honeycomb lattice system and its electrochemical analysis for the detection of sulfadiazine. *J. Chem. Eng.* **464**, 142673 (2023)
 38. T.S.K. Sharma, K. Hwa, Architecting hierarchal Zn₃V₂O₈/P-rGO nanostructure: Electrochemical determination of anti-viral drug azithromycin in biological samples using SPCE. *J. Chem. Eng.* **439**, 135591 (2022)
 39. M. Tezerjani, A. Benvidi, A. Firouzabadi, M. Ardakani, A. Akbari, Epinephrine electrochemical sensor based on a carbon paste electrode modified with hydroquinone derivative and graphene oxide nano-sheets: simultaneous determination of epinephrine, acetaminophen and dopamine. *Meas.* **101**, 183–189 (2017)
 40. F. Cui, X. Zhang, Electrochemical sensor for epinephrine based on a glassy carbon electrode modified with graphene/gold nanocomposites. *J. Electroanal. Chem.* **669**, 35–41 (2012)
 41. S. Leau, C. Lete, C. Matei, S. Lupu, Electrochemical sensing platform based on metal nanoparticles for epinephrine and serotonin. *Biosens.* **13**, 781 (2023)
 42. M. Ardakani, F. Yazdi, F. Dokht, A. Khoshroo, Fabrication of an Electrochemical Sensor for Determination of Epinephrine Using a Glassy Carbon Electrode Modified with Catechol. *Anal. Bioanal. Chem. Res.* **10**, 387–394 (2023)
 43. K. Reddy, M. Satyanarayana, K. Goud, K. Gobi, H. Kim, Carbon nanotube ensembled hybrid nanocomposite electrode for direct electrochemical detection of epinephrine in pharmaceutical tablets and urine. *Mater. Sci. Eng. C* **79**, 93–99 (2017)
 44. T. Tsai, S. Thiagarajan, S. Chen, C. Cheng, Ionic liquid assisted synthesis of nano Pd–Au particles and application for the detection of epinephrine, dopamine and uric acid. *Thin Solid Films* **520**, 3054–3059 (2012)
 45. K. Sen, S. Ali, D. Singh, K. Singh, N. Gupta, Development of metal free melamine modified graphene oxide for electrochemical sensing of epinephrine. *FlatChem* **30**, 100288 (2021)
 46. H. Madhuchandra, B. Swamy, Electrochemical determination of Adrenaline and Uric acid at 2-Hydroxybenzimidazole modified carbon paste electrode Sensor: a voltammetric study. *Mater Sci Energy Technol* **3**, 464–471 (2020)
 47. X. Yang, P. Zhao, Z. Xie, M. Ni, C. Wang, P. Yang, Y. Xie, J. Fei, Selective determination of epinephrine using electrochemical sensor based on ordered mesoporous carbon/nickel oxide nanocomposite. *Talanta* **233**, 122545 (2021)

Publisher's Note Springer Nature remains neutral with regard to jurisdictional claims in published maps and institutional affiliations.